Formation of Polycrystalline Microparticles from Evaporating Fine Droplets of Aqueous NaCl Solution

Alexander A. Fedorets , Anna V. Nasyrova , Vladimir Yu. Levashov , Andrey N. Bobylev , Leonid A. Dombrovsky *

Posted Date: 22 April 2026

doi: 10.20944/preprints202604.1608.v1

Keywords: saltwater droplets; evaporation; polycrystalline salt particles; experimental study

 doi:10.20944/preprints202604.1608.v1

Article

Formation of Polycrystalline Microparticles from Evaporating Fine Droplets of Aqueous NaCl Solution

Alexander A. Fedorets [1], Anna V. Nasyrova [1], Vladimir Yu. Levashov [2], Andrey N. Bobylev [1] and Leonid A. Dombrovsky [1,3,*]

[1] X-BIO Institute, University of Tyumen, 6 Volodarskogo St, Tyumen, 625003, Russia
[2] Institute of Mechanics, Lomonosov Moscow State University, Moscow, 119991, Russia
[3] Faculty of Engineering, Ariel University, Ariel, 407000, Israel
* Correspondence: ldombr@yandex.ru

Abstract

The fall of droplets of an aqueous NaCl solution in a vertical channel, filled with heated dry air, is studied. Water from the droplets evaporates quickly, and crystals of a solid salt crust form on their surface. At a later stage of the process, the remaining solution is removed from the droplet using a jet of water vapor that passes through the pores of the polycrystalline crust. It was first observed that some of the drying droplets suddenly shifted to one side under the influence of the reactive force generated by the vapor jet. The resulting salt particles are weakly porous and consist of many crystals. It has been proven that these particles don't have a central cavity. The use of seawater and the role of salt particles in protecting against thermal radiation from fires are briefly discussed. Calculations based on Mie theory have shown that the contribution of light scattering by hollow sea salt particles formed above the ocean surface during relatively slow evaporation of seawater droplets can be significant in the ocean's heat balance.

Keywords: saltwater droplets; evaporation; polycrystalline salt particles; experimental study

1. Introduction

The study of the evaporation of small droplets of aqueous solutions of non-volatile substances is of interest for solving a wide variety of problems. For example, such droplets are used in the pharmaceutical industry to produce medicinal powders [1–9] and in seawater desalination [10–13]. Mist curtains containing seawater droplets are used to protect against the thermal radiation of fires [14,15]. The evaporation of pesticide droplets on plants' roots or leaves will affect their insecticidal effect [16–20]. Controlling the evaporation of saline droplets is important for indoor air quality and reducing energy consumption in buildings [21,22]. The evaporation of seawater droplets above the sea surface affects the interaction between the ocean and the lower atmosphere [23–27].

The presence of a nonvolatile substance in a water droplet significantly complicates the physical picture of droplet evaporation. Due to the slow diffusion of the dissolved substance, water evaporation increases the concentration of that substance near the droplet surface, and the subsequent formation of a solid crust further hinders evaporation. As a result of the increase in pressure, water vapor can penetrate the structure of the polycrystalline shell, and the remaining solution is jetted out of the particle. Interestingly, the resulting solid particles may have a complex crystalline structure that depends on the temperature and relative humidity of the surrounding air.

The process described above is known. References to relevant studies can be found in both review articles [1,28–33] and regular papers [34–48]. Some of the cited works examine the influence of dissolved sodium chloride on water droplet evaporation. These papers are most relevant to the present study. As usual, the low diffusivity of sodium chloride in water [49–51] leads to a rapid increase in salt concentration at the evaporation surface and a significant decrease in the evaporation rate of the aqueous solution [52,53].

 doi:10.20944/preprints202604.1608.v1

In the present work, laboratory studies of the formation of crystalline sodium chloride microparticles from saltwater droplets surrounded by dry hot air are continued. Based on the observed sharp decrease in the falling speed of the evaporating droplet and the deviation of its trajectory from the vertical, the escape of water vapor and the remaining concentrated salt solution through a side opening in the polycrystalline shell was detected. It has been established that this effect occurs just before the formation of a rather dense polycrystalline particle.

2. Laboratory Set-Up and Experimental Procedure

The experiments were conducted using droplets of an aqueous sodium chloride solution. The concentration of the solution was equal to $c_{\text{salt}} = 35 \pm 0.5$ g/l, which corresponds to the average concentration of salts in seawater. As in a recent article [54], a complex stream of polydisperse droplets generated by a dispenser was converted into a flow of falling droplets with diameters of 90–100 μm in the air-filled vertical channel. This was achieved using the design shown in Figure 1, where "1" denotes a cylindrical plastic housing containing an ultrasonic dispenser from Altrasonic (China). This housing of inner diameter 38 mm is connected to a vertical channel "2" with a square cross-section of 20 mm × 20 mm. The vertical channel acts as a simple and effective filter, retaining only drops of nearly identical, specified size from the polydisperse droplets generated by the dispenser, which have a wide size distribution.

Figure 1. The image of the experimental set-up.

In [48], calculations were carried out which helped to determine the required distance between the dispenser and the axis of the long vertical channel. The viscous drag force stabilizes the droplet fall velocity. This velocity changes only because of the droplet's gradual evaporation. Note that the vertical channel used in the present paper is much longer than that in [54] because we were going to obtain hollow or dense crystalline particles from the droplets of aqueous solution of sodium chloride. To promote the droplets' evaporation, the air in the vertical channel was heated using a heat gun R858D (REXANT, Russia) "3". To monitor air temperature and humidity in the experiment, the digital thermometer HI98501 (HANNA Instruments, Germany) and the thermohygrometer IVTM-7 M K (Exis, Russia) were used. Measurements showed that, during the experiment, the air

 doi:10.20944/preprints202604.1608.v1

temperature and humidity remained constant throughout the entire channel. The following values for air temperature and relative humidity were selected as the operating conditions: $T = 60 \pm 1$℃ and $\varphi = 30 \pm 1\%$. The stability of the temperature and relative humidity was monitored through measurements taken during the experiment. These conditions, as in [43,44,47], allow the setup to be relatively compact but lead to more rapid water evaporation from the droplets and the formation of a polycrystalline salt crust on the surface of small droplets containing a more concentrated solution. At the bottom of the vertical channel, there were glass windows (w) measuring 20 mm × 60 mm, which allowed the falling particles to be illuminated and observed. The channel ended with a removable plug "4", into which a glass plate was placed during the experiment. Salt particles that fell onto the plate were examined using scanning electron microscopy (SEM) after the experiment. An LED light source "5" (Logocam, LED BM-50 V 3200/5600, Israel) was used for video recording by a high-speed camera "6" (Photron FASTCAM NOVA, Japan) equipped with a lens AF-S VR Micro-NIKKOR 105mm f/2.8G (Nikon, Japan). The length of the evaporating droplet's trajectory in the channel to the upper edge of the camera's field of view was approximately 46 cm. This study focuses on the final stage of water evaporation, when a solid crystalline particle is forming.

High-speed (5000 fps) photography of falling particles was performed at the final part of the trajectory, approximately 3 cm from the surface of the glass plate. Under these conditions, the microdroplets had time to dry during their fall and landed on the plate surface as salt particles. The microsphere samples were examined using a MIRA3 scanning electron microscope (TESCAN, Czech Republic). Before this procedure, the samples on a glass substrate were coated with a 20 nm thick gold layer using a Q150R S automatic magnetron sputtering system (Quorum Technologies, UK).

3. Experimental Results

Most of the evaporating and partially solidified droplets, whose trajectories are recorded using a high-speed camera, move downwards. Since the size of these particles is approximately half that of the droplets of aqueous solutions whose fall was considered in [54], the viscous drag force of air is well described by Stokes' law. This statement is confirmed by the typical value of the Reynolds number for a spherical particle with a diameter d falling in an immovable gas at a certain velocity v_p:

$$\mathrm{Re_p} = \rho_\mathrm{air} v_\mathrm{p} d / \eta_\mathrm{air}, \quad (1)$$

where ρ_air and η_air are the density and dynamic viscosity of surrounding air. Assuming $\rho_\mathrm{air} = 1.06$ kg/m^3, $\eta_\mathrm{air} = 1.97 \cdot 10^{-5}$ Pa s, and $d = 25$ μm for the experimental conditions, with a typical equilibrium particle fall velocity $v_\mathrm{p} = 60$ mm/s (upper estimate), we obtain $\mathrm{Re_p} \approx 0.08$. Such a low Reynolds number means that Stokes' formula for the drag coefficient $C_D = 24/\mathrm{Re_p}$ is applicable for spherical particles [55,56]. The condition of equilibrium between gravitational force and drag force leads to the following equation for the equilibrium velocity of a spherical salt particle with a conventional porosity p, which may be a real porosity or a relative volume of the central cavity (in the case of hollow particle with a dense salt shell):

$$v_\mathrm{p} = \frac{\rho_\mathrm{salt}(1-p)}{18\eta_\mathrm{air}} g d^2, \quad (2)$$

where $\rho_\mathrm{salt} = 2173$ kg/m^3 is the density of salt crystals and $g = 9.81$ m/s^2 is the acceleration of gravity. One might decide that the value of p can be determined from Eq. (2). However, it will be shown below that this is not the case due to the very low porosity and slightly non-spherical shape of many particles.

It is interesting to note those drops whose trajectories deviate slightly from the vertical for a brief moment. These deviations are due to the escape of vapor and solution residues through the pores in the polycrystalline salt structure. As the depth of field of the high-speed camera's lens is quite shallow, only a few droplets are clearly visible over a significant part of the trajectory. One of these successful observations of a droplet, whose trajectory deviates from the vertical, is shown in Figure 2. It should be noted that this sudden deviation is observed in only one of the droplets in the group. The other droplets nearby continue to fall strictly vertically. This means that the change in the

 doi:10.20944/preprints202604.1608.v1

droplet's trajectory in question cannot be explained by a disturbance in the air flow, which would inevitably have affected the entire group of nearby droplets.

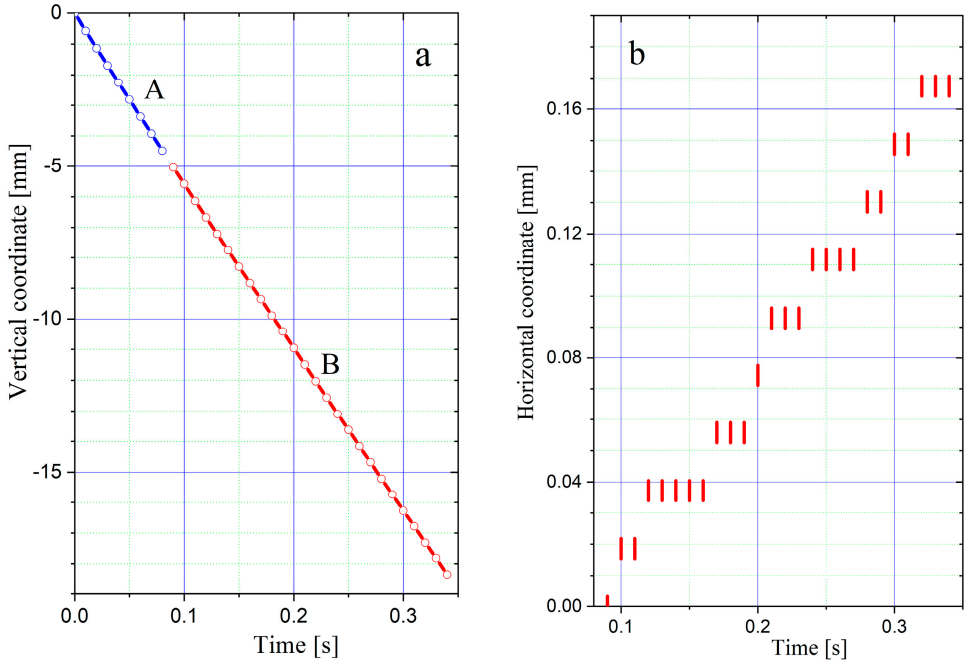

Figure 2. a – downward motion of the droplet: A – with a velocity v_{p1} before the lateral force is applied, B – with a velocity $v_{p2} < v_{p1}$ after this force is applied; **b** – lateral motion of the droplet.

A small but sharp decrease in the drop's falling speed at a conventional moment in time $t_* = 0.08 - 0.09$ s is shown in Figure 2a. The vertical component of the droplet velocity (in direction of z-axis) is constant for both $t < t_*$ and $t > t_*$, but the velocity value changes from $v_{p1} = 56$ mm/s to $v_{p2} = 53$ mm/s for $t > t_*$. The decrease in the droplet falling velocity is due to mass losses after the remaining concentrated solution has escaped from the droplet along with the vapor. The horizontal motion of the droplet at $t > t_*$ is shown in Figure 2b. The vertical segments instead of dots are reminiscent of the rather large pixels of an image obtained with a digital camera. As shown in Figure 2b, the horizontal velocity u_p of the particle is equal to zero during the initial time interval of $\Delta t \approx 0.1$ s. After that, the velocity first increases, but then decreases and remains almost constant, at least for 0.3 s. This result can be explained by the fact that the mass flow rate of steam with solution residues continues throughout this time.

Several SEM images of the obtained salt particles were taken. All particles consisted of nearly identical large sodium chloride crystals. Two of these images are shown in Figure 3. The shape of the particle in Figure 3a appears to be the closest to spherical. For Figure 3b, a particle was selected whose shape differed most significantly from a sphere. Nevertheless, the asymmetry of even this second particle does not appear to be significant. This means that the drag force for asymmetrical particles may be only slightly greater than for a spherical particle. The shape of the small salt particles cannot change when they settle on the glass substrate. This happened whilst the particles were falling.

Returning to the relationship between salt particle size and their falling velocity, we can substitute several particle diameter values into Eq. (2), assuming that the particles are non-porous. Simple calculations give $v_p = 37.5$ mm/s at $d = 25$ μm and $v_p = 54$ mm/s at $d = 30$ μm. Based on a comparison of these results and the measured values $v_{p1} = 56$ mm/s and $v_{p2} = 53$ mm/s, two important conclusions can be drawn: (1) The drag coefficient of salt particles is greater than that of a smooth sphere, (2) The particles have no central hole, and the conventional volumetric porosity of salt particles is negligibly small. The latter statement enables us to estimate the initial diameter of droplets in the cross-section of the inlet of the vertical channel:

 doi:10.20944/preprints202604.1608.v1

$$d_0 = d/\sqrt[3]{c_{\text{salt}}}. \quad (3)$$

Equation (3) gives $d_0 = 94$ μm at $d = 30$ μm. This is consistent with the values for the initial diameter, approximately 90–100 μm, reported in [54]. This implies that evaporation of the droplet before it reaches the vertical channel is negligible, even in the heated air.

It should be noted that the experimental results of this work were obtained at unusually high temperatures and low relative humidity of the surrounding air. Such conditions are rare in nature and technology. As a rule, droplets of aqueous sodium chloride solution or seawater do not evaporate so quickly. In this case, thin-walled hollow salt particles are indeed formed, the size of which is not much smaller than the size of the initial solution droplets [29,32–42,45,46].

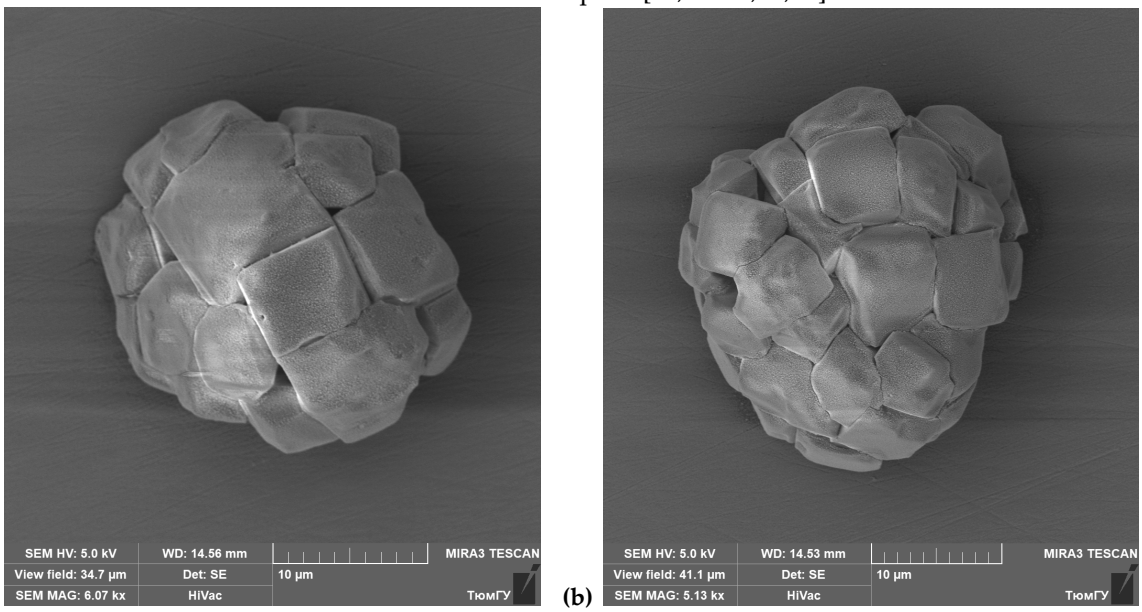

Figure 3. SEM images of salt particles: **(a)** – almost spherical particle, **(b**) – asymmetric particle. Sodium chloride crystals and some gaps between them are visible.

4. Some Applications

The formation of solid hollow particles during the evaporation of droplets of aqueous solutions of non-volatile substances is not only of academic interest. Such particles, formed from seawater droplets in water mist curtains, are used to shield against thermal radiation of large flames during fires [14,15]. Unfortunately, in some coastal regions, as well as on seagoing ships and oil platforms, there is no access to fresh water. Therefore, in [14,15], a study was conducted on the possible use of seawater. It was shown that the infrared optical properties of hollow salt shells, which are formed from seawater droplets in the lower part of a mist curtain, contribute sufficiently to the attenuation of the infrared radiation of real large fires.

It turns out that the optical properties of hollow salt particles in the visible and near-infrared spectral ranges are also favorable for the thermal regime of the ocean. These particles formed from water sprays can protect the ocean from excessive heating by solar radiation. To justify this statement, let us compare the calculated values of the transport efficiency factor of scattering $Q_{\text{s}}^{\text{tr}} = Q_{\text{s}} \times (1 - \bar{\mu})$, where Q_{s} is the ordinary efficiency factor of scattering and $\bar{\mu}$ is the asymmetry factor of scattering [57–60], for the seawater droplet and the corresponding hollow sea-salt particle. For known spectral optical properties of substances, calculations can be performed using the Mie theory for homogeneous and hollow spherical particles, as described in [14]. The independent scattering hypothesis can be applied to these randomly distributed droplets and particles, as their sizes and the distances between them are generally much greater than the wavelength of solar radiation [61–63]. Of course, the evaporation of sea water droplets in the air near the ocean surface occurs much more slowly than in the laboratory setup described above, where the air is preheated. Therefore, the evaporation of water results in hollow salt particles that are only slightly smaller than the original

 doi:10.20944/preprints202604.1608.v1

seawater droplets. The results of calculations for a droplet with a diameter of 100 μm and a hollow spherical sea-salt particle with a diameter of 80 μm and shell thickness $\delta = 0.1$ μm are shown in Figure 4. Note that the mass of salt in the selected hollow salt particle is approximately the same as in the original droplet of seawater. It can be seen that a hollow salt particle scatters solar spectrum radiation several times more strongly than a droplet of seawater from which such a particle is formed during evaporation. This means that a horizontal curtain of hollow sea salt particles can make a considerable contribution to the attenuation of solar radiation reaching the sea surface. The effect described should be taken into account when calculating the heat balance of the ocean and atmosphere.

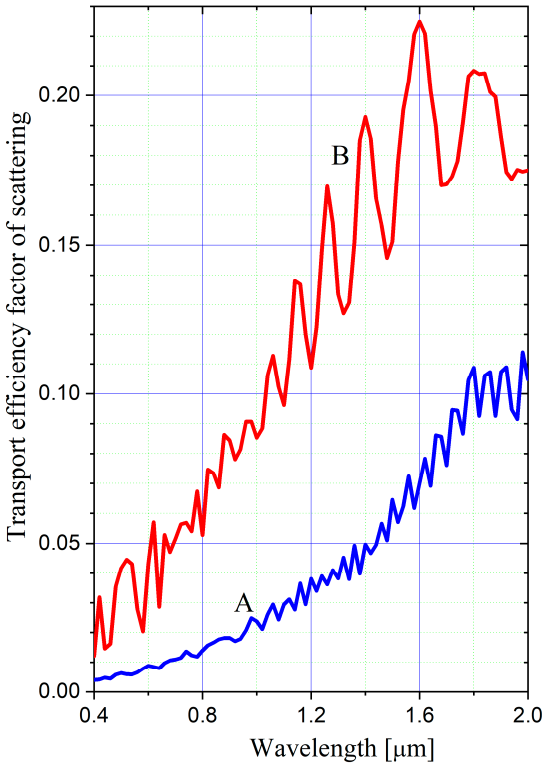

Figure 4. Transport efficiency factor of scattering in the visible and near-infrared spectral ranges: (A) seawater droplet with a diameter of 100 μm and (B) hollow sea-salt particles with an external diameter of 80 μm.

5. Conclusions

The processes of evaporation and crystallization of droplets of an aqueous sodium chloride solution were investigated as the droplets fell through a vertical channel filled with heated dry air. The initial salt concentration in the droplets is close to typical seawater values. At an ambient temperature of around 60 °C, the water evaporates rapidly, and salt crystals begin to form on the droplet surface. At a later stage of the process, due to the water vapor pressure, the remaining solution is removed through the pores of the solidifying polycrystalline salt particle. For the first time, it was observed that some droplets undergoing drying suddenly began to shift sideways under the action of the reactive force created by the vapor jet. The prolonged vertical fall of such particles slows down due to the loss of a small part of their mass. The resulting salt particles are slightly porous and consist of many large crystals. This is clearly visible in SEM images of particles and is consistent with measurements of the particle fall velocity. Some applications of hollow salt particles obtained by less intense heating are discussed. Calculations based on Mie theory have shown that the contribution of light scattering by hollow sea-salt particles forming above the ocean surface may be considerable in the ocean's heat balance.

 doi:10.20944/preprints202604.1608.v1

Author Contributions: Conceptualization, methodology, design of the experimental set-up and experimental study – A.A.F.; Conceptualization and writing the paper – L.A.D.; Design of the experimental set-up and measurements – A.V.N., methodology and theoretical estimates – V.Yu.L.; Experimental methodology, SEM microscopy – A.N.B. All the authors have read and agreed to the published version of the manuscript.

Funding: This research was funded by the Russian Science Foundation (project no. 24-29-00303).

Acknowledgments: The authors are grateful to the Russian Science Foundation (project no. 24-29-00303).

Conflicts of Interest: The authors declare no conflict of interest.

References

1. Vehring, R. Pharmaceutical particle engineering via spray drying. *Pharm. Res.* **2008**, 25(5), 999–1022.
2. Katon, H.; Wandrey, A.J.; Gander, B. Kinetics of solvent extraction/evaporation process for PLGA microparticle fabrication. *Int. J. Pharmaceut.* **2008**, 364, 45–53.
3. Van Eedenbrugh, B.; Baird, J.A.; Taylor, L.S. Cystallization tendency of active pharmaceutical ingredients following rapid solvent evaporation – classification and comparison with crystallization tendency from undercooled melts. *J. Pharmaceut. Sci.* **2010**, 99(9), 3826–3838.
4. Iqbal, M.; Zafar, N.; Fessi, H.; Elaissari, A. Double emulsion solvent evaporation techniques used for drug encapsulation. *Int. J. Pharmaceut.* **2015**, 462(2), 179–190.
5. Zang, D.; Tarafdar, S.; Tarasevich, Yu.Yu.; Choudhurry, M.D.; Dutta, T. Evaporation of a droplet: From physics to applications. *Phys. Rep.* **2019**, 804, 1–56.
6. Ziaee, A.; Albadarin, A.B.; Padrela, L.; Femmer, T.; O'Reilly, E.; Walker, G. Spray drying of pharmaceuticals and biopharmaceuticals: Critical parameters and experimental process optimization approaches. *Eur. J. Pharm. Sci.* **2019**, 127, 300–318.
7. Korornaczyk, M.O.; Würtenberger, S.; Baumgartner, S. Impact of succussion on pharmaceutical preparations analysed by means of patterns from evaporated droplets. *Sci. Rep.* **2020**, 570.
8. Boel, E.; Koerjekx, R.; Dedroog, S.; Babkin, I.; Vetrano, M.R. et al. Unravelling particle formation: From single droplet drying to spray drying and electrospraying. *Pharmaceutics* **2020**, 12, 625.
9. Baumann, J.M.; Adam, M.S.; Wood, J.D. Engineering advances in spray drying for pharmaceuticals. *Annu. Rev. Chem. Biomol. Eng.* **2021**, 12, 217–240.
10. Chen, Q.; Thu, K.; Bui, T.D.; Li, Y.; Ng, K.C.; Chua, K.J. Development of a model for spray evaporation based on droplet analysis. *Desalination* **2016**, 399, 69–77.
11. Chen, Q.; Kum, Ja.M.; Li, Y.; Chua, K.J. Experimental and mathematical study of the spray flash evaporation phenomena. *Appl. Therm. Eng.* **2018**, 130, 598–610.
12. Dong, C.; Huang, Y.; Zhang, L. Slug flow-enhanced vacuum membrane distillation for seawater desalination: Flux improvement and anti-fouling effect. *Sep. Purif. Tech.* **2023**, 320, 124178.
13. Li, A.; He, M.; Zheng, M.; Liu, H.; Liu, Y. et al. Bioinspired multi-scale core-spun yarn-based solar evaporator for ultra-efficient and durable high-salinity brine desalination. *Fundam. Res.* **2025**, 1144–1152.
14. Dombrovsky, L.A.; Levashov, V.Yu.; Kryukov, A.P.; Dembele, S.; Wen, J.X. A comparative analysis of shielding of thermal radiation of fires using mist curtains containing droplets of pure water or sea water. *Int. J. Therm. Sci.* **2020**, 152, 106299.
15. Dombrovsky, L.A.; Dembele, S. An improved solution for shielding of thermal radiation of fires using mist curtains of pure water or seawater. *Comput. Therm. Sci.* **2022**, 14(4), 1–18.
16. Zhou, Z.; Cao, C.; Cao, L.; Zheng, L.; Xu, J. et al. Evaporation kinetics of surfactant solution droplets on rice (*Oryza sativa*) leaves. *PLOS One* **2017**, 12, e0176870.
17. Zhou, Z.; Cao, C.; Cao, L.; Zheng, L.; Xu, J. et al. Effect of surfactant concentration on the evaporation of droplets on cotton (*Gossypium hirsutum L.*) leaves. *Colloids Surf. B* **2018**, 167, 206–212.
18. Li, H.; Cryer, S.; Raymond, J.; Acharya, L. Interpreting atomization of agricultural spray image patterns using latent Dirichlet allocation techniques. *Art. Intel. Agric.* **2020**, 4, 253–261.
19. Gao, K.; Haddad, S.; Paolini, R.; Feng, J.; Altheeb, M. et al. The use of green infrastructure and irrigation in the mitigation of urban heat in a desert city. *Build Simul.* **2024**, 17, 679–694.

 doi:10.20944/preprints202604.1608.v1

20. Lankinen, Å.; Witzell, J.; Aleklett, K.; Furenhed, S.;·Green, K.K. et al. Challenges and opportunities for increasing the use of low-risk plant protection products in sustainable production. A review. *Agron. Sustain. Dev*. **2024**, 44, 21.
21. Wang, Y.; Zou, Y.; Yang, Y.; Wu, S.; Zhang, X.; Ren, X. Movement and control of evaporating droplets released from an open surface tank in the push–pull ventilation system. *Build Simul.* **2016**, 9, 443–457.
22. Duverge, J.J.; Rajagopalan, P. Assessment of factors influencing the energy and water performance of aquatic centres. *Build Simul.* **2020**,13, 771–786.
23. Shahidzadeh, N.; Schut, M.F.L.; Desarnaud, J.; Prat, M.; Bonn, D. Salt stains from evaporating droplets. *Sci. Rep.* **2015**, 5, 10355.
24. Chi, J.W.; Li, W.J.; Zhang, D.Z.; Zhang, J.C.; Lin, Y.T. et al. Sea salt aerosols as a reactive surface for inorganic and organic acidic gases in the Arctic troposphere. *Atmos. Chem. Phys.* **2015**, 15, 11341–11353.
25. Schiffer, J.M.; Mael, L.E.; Prather, K.A.; Amaro, R.E.; Grassian, V.H. Sea spray aerosols: Where marine biology meets atmospheric chemistry. *ACS Cent. Sci.* **2018**, 4(12), 1617–1623.
26. Brian, H.; Froyd, K.; Murphy, D.M.; Dibb, J.; Darmenov, A. et al. Observationally constrained analysis of sea salt aerosols in the marine atmosphere. *Atmos. Chem. Phys.* **2019**, 19(16), 10773–10785.
27. Ackerman, K.L.; Nugent, A.D.; Taing, C. Mechanisms controlling giant sea salt aerosols size distributions along a tropical orographic coastline. *Atmos. Chem. Phys.* **2023**, 23(21), 13735–13753.
28. Walton, D.E.; Mumford, C.J. The morphology of spray-dried particles: The effect of process variables upon the morphology of spray-dried particles. *Chem. Eng. Res. Des.* **1999**, 77(5), 442–460.
29. Vehring, R.; Foss, W.R.; Lechuga-Ballesteros, D. Particle formation in spray drying. *Aerosol Sci.* **2007**, 38(7), 728–746.
30. Nandiyanto, A.B.D.; Okuyama, K. Progress in developing spray-drying methods for the production of controlled morphology particles: From the nanometer to submicrometer size ranges. *Adv. Powder Tech.* **2011**, 22(1), 1–19.
31. Sadek, C.; Schuck, P.; Fallourd, Y.; Pradeau, N.; Le Froch-Fouéré, C.; Jeantet, R. Drying of a single droplet to investigate process–structure–function relationships: a review. *Dairy Sci. Tech.* **2015**, 95, 771–794.
32. De Souza Lima, R.; Ré, M.-I.; Arlabosse, P. Drying droplet as a template for solid formation: A review. *Powder Tech.* **2020**, 359:161–171.
33. Dombrovsky, L.A.; Levashov, V.Yu.; Shoval, S.; Bormashenko, Ed. Progress in understanding of evaporation of droplets: Fundamentals and applications. *Adv. Coll. Interface Sci.* **2025**, 344, 103605.
34. Cheng, R.G.; Blanchard, D.C.; Cipriano, R.J. The formation of hollow sea-salt particles from the evaporation of drops of seawater. *Atmos. Res.* **1988**, 22(1), 15–25.
35. Handscomb, C.S.; Kraft, M.; Bayly, A.E. A new model for the drying of droplets containing suspended solids after shell formation. *Chem. Eng. Sci.* **2009**, 64 (2), 228–246.
36. Handscomb, C.S.; Kraft, M.; Bayly, A.E. A new model for the drying of droplets containing suspended solids. *Chem. Eng. Sci.* **2009**, 64 (4), 628–637.
37. Fairhurst, D. Droplets of ionic solutions, Chap. 20 in "*Droplet Wetting and Evaporation. From Pure to Complex Fluids*" ed. by D. Brutin, Acad. Press, New York, **2015**, 295–313.
38. Mezhericher, M.; Levi, A.; Borde, I. Multi-scale multiphase modeling of transport phenomena in spray-drying processes. *Drying Tech.* **2015**, 33(1), 2–23.
39. Quilaquero, M.; Aguilera, J.M.; Crystallization of NaCl by fast evaporation of water droplets of NaCl solutions. *Food Res. Int.* **2016**, 84, 143–149.
40. Gregson, F.K.A.; Robinson, J.F.; Miles, R.E.H.; Royall, C.P.; Reid, J.P. Drying kinetics of salt solution droplets: Water evaporation rates and crystallization. *J. Phys. Chem. B* **2019**, 123(1), 266–276.
41. Nandiyanto, A.B.D.; Ogi, T.; Wang, W.-N.; Gradon, L.; Okuyama, K. Template-assisted spray-drying method for the fabrication of porous particles with tunable structures. *Adv. Powder Tech.* **2019**, 30(12), 2908–2924.
42. Rezaei, M.; Netz, R.R. Water evaporation from solute-containing aerosol droplets: Effects of internal concentration and diffusivity profiles and onset of crust formation. *Phys. Fluids* **2021**, 33, 091901.

 doi:10.20944/preprints202604.1608.v1

43. Hardy, D.A.; Archer, J.; Lemaitre, P.; Vehring, R.; Reid, J.P.; Walker, J.S. High time resolution measurements of droplet evaporation kinetics and particle crystallization. *Phys. Chem. Chem. Phys.* **2021**, 23(34), 18568−18579.
44. Hardy, D.A.; Robinson, J.F.; Hilditch, T.G.; Neal, E.; Lemaitre, P.; Walker, J.S.; Reid, J.P. Accurate measurements and simulations of the evaporation and trajectories of individual solution droplets. *J. Phys. Chem. B* **2023**, 127(15), 3416−3430.
45. O'Connell, K.; Olaleye, A.K.; Van den Akker, H.E.A. A porous-crust drying model for a single dairy droplet. *Chem. Eng. Res. Des.* **2023**, 200, 741–752.
46. Licsandru, G.; Noiriel, C.; Duru, O.; Geoffroy, S.; Abou-Chakra, A.; Prat, M. Evaporative destabilization of a salt crust with branched pattern formation. *Sci. Rep.* **2023**, 13, 5132.
47. Miles, B.E.A; Winter, E.; Mirembe, S.; Hardy, D.; Mahato, L.K.; Miles, R.E.H.; Reid, J.P. Evaporation kinetics and final particle morphology of multicomponent salt solution droplets. *J. Phys. Chem. A* **2025**, 129(3), 762–773.
48. Mignot, B.; Mahmud, T.; Heggs, P.J.; Ghadiri, M.; Roberts, K.J. Modelling and experimental validation of the evaporation and crystallization of a saline droplet. *Chem. Eng. Sci.* **2026**, 322, 123114.
49. Wang, J.; Fiebig, M. Absolute measurements of the thermal diffusivity of aqueous solutions of sodium chloride. *Int. J. Thermophys.* **1998**, 19(1):15–25.
50. Hamann, C.H.; Hamnett, A.; Vielstich, W. *Electrochemistry. Second Edition*; Wiley: Weinheim, Germany, **2007**.
51. Zhang, J.; Clennell, M.B.; Dewhurst, D.N. Transport properties of NaCl in aqueous solution and hydrogen solubility in brine. *J. Phys. Chem. B* **2023**, 127, 8900–8915.
52. Fedorets, A.A.; Shcherbakov, D.V.; Levashov, V.Yu.; Dombrovsky, L.A. Self-stabilization of droplet clusters levitating over heated salt water. *Int. J. Therm. Sci.* **2022**, 182, 107822.
53. Fedorets, A.A.; Kolmakov, E.E.; Dombrovsky, L.A. Experimental study of the effect of water salinity on the parameters of an equilibrium droplet cluster levitating over a water layer. *Front. Heat Mass Transfer* **2024**, 22(1), 1–14.
54. Fedorets, A.A.; Kolmakov, E.E.; Nasyrova, A.V.; Medvedev, D.N.; Mayorov, V.O.; Levashov, V.Yu.; Dombrovsky, L.A. Experimental method for studying the effect of dissolved substances on the evaporation rate of water droplets suspended in air. *Front. Heat Mass Transfer* **2025**, 24(4), 1091–1102.
55. Goossens, W.R.A. Review of the empirical correlations for the drag coefficient of rigid spheres. *Powder Tech.* **2019**, 352, 350–359.
56. Singh, N.; Kroells, M.; Li, C.; Ching, E.; Ihme, M.; Hogan, C.J.; Schwartzentruber, T.E. General drag coefficient for flow over spherical particles. *AIAA J.* **2022**, 60(2), 587–597.
57. Van de Hulst, H.C. *Light Scattering by Small Particles*; Dover: New York, USA, **1981**.
58. Bohren, C.F.; Huffman, D.R. *Absorption and Scattering of Light by Small Particles*; Wiley: New York, USA, **1998**.
59. Mishchenko, M.I.; Travis L.D.; Lacis, A.A. *Multiple Scattering of Light by Particles: Radiative Transfer and Coherent Backscattering*; Cambridge University Press: Cambridge (UK), **2006**.
60. Dombrovsky, L.A.; Baillis, D. *Thermal Radiation in Disperse Systems: An Engineering Approach*; Begell House: New York, USA, **2010**.
61. Mishchenko, M.I. Electromagnetic Scattering by Particles and Particle Groups: An Introduction; Cambridge University Press: New York, USA, **2014**.
62. Mishchenko, M.I. "Independent" and "dependent" scattering by particles in a multi-particle group. *OSA Continuum* **2018**, 1(1), 243–260.
63. Galy, T.; Huang, D.; Pilon, L. Revisiting independent versus dependent scattering regimes in suspensions or aggregates of spherical particles. *J. Quant. Spectr. Radiat. Transfer* **2020,** *246*, 106924.